

Progress of experimental and numerical modelling study on low-low temperature electrostatic precipitators

Jun Guo¹, Ding Yang¹, Baoyu Guo², Yinbiao Su¹, Xinglian Ye¹, Aibing Yu², Shuiqing Li³

¹ Fujian Longking Co., Ltd., Longyan, Fujian 36400, China

² School of Mat. Sci. and Eng., University of New South Wales, NSW 2052, Australia

³ Faculty of Mechanical Eng., Tsinghua University, Beijing 100084, China

Corresponding author: junguo318@139.com

Abstract Low-low temperature ESPs are important flue gas control device in the near future to achieve ultra-low emission from coal-fired power plant in China. In order to reveal the dust removal mechanism and performance-affecting factors of ESP, Fujian Longking Co., Ltd. has carried out considerable research work, including experimental tests under laboratory and engineering conditions, and numerical modelling of LLTESP. In the experimental study of LLTESP, the effect of temperature on the dust resistivity, grade removal efficiency and charge quantity under laboratory and engineering conditions are described in detail. The test results indicate that, as the flue gas temperature is reduced, dust resistivity decreases, grading dust removal efficiency and charging quantity are promoted, enhancing significantly the dust removal efficiency of ESP in engineering applications. In the numerical part, the history of numerical simulation of electrostatic precipitators, technical progress and existing problems are reviewed. The main methods of numerical simulations and the progress of current work are described in details, and the numerical modelling results are analysed. Studies have shown that LLTESP has a significant effect on improving ESP through reduced dust resistivity and increased working voltage. Sulfuric acid condensation can increase the particle saturation charge by an increase in effective dielectric constant of dust particles. The decrease of flue gas temperature changes air density, viscosity, dust resistivity, electric field and acid deposition conditions, thereby enhancing the efficiency of electrostatic precipitators.

Keywords: Low-low temperature ESP, working mechanism, collection efficiency, numerical simulation

1. Background

ESP is now a dominating technology for coal-firing power plants for its advantage in high dust removal efficiency, low pressure drop, high flue gas handling capacity, low operation costs and no secondary pollution [1]. ESP collection performance is sensitive to dust resistivity, with desired value of $10^4 \sim 10^{11}$ Ωcm . Typical ESPs operate at $120^\circ\text{C} \sim 150^\circ\text{C}$. Over this range, dust resistivity is higher and electric charges on the dust particles collected do not release easily, so rapping intensity must be enhanced, resulting in dust re-entrainment. Meanwhile, when the dust resistivity rises to some point, the back corona phenomena occur, which sharply deteriorate ESP efficiency.

Dust resistivity can be reduced from a temperature perspective in two ways: 1) increasing operating temperature of electric precipitator; 2) reducing electrostatic precipitators operating temperature. This idea has formed two types of electrostatic precipitators. Elevated ESP operating temperature can decrease the volume resistivity, subsequently the total resistivity of dust. Based on this principle, a hot side ESP was developed. During 1960s ~1980s the United States built many hot-side ESPs, which were placed in front of air preheater in coal-fired power plant with an operating temperature of $300^\circ\text{C} \sim 450^\circ\text{C}$. Due to various drawbacks, however, this type of ESPs are now rarely used. Reducing ESP operating temperature (generally decreased from $120^\circ\text{C} \sim 150^\circ\text{C}$ to around 90°C), can make the surface resistivity of dust thus the dust layer

resistivity decrease. Based on this principle, low-low temperature ESP was developed [2, 3].

2. Low-low temperature ESP technology

Low-low temperature ESP (Called in China according to JB/T 12591-2016, LLTESP for short) utilizes low temperature coal economizer or gas-gas heat exchanger (GGH) with water as a medium to recover residual heat from flue gas. The flue gas can be cooled down to a low temperature state of 90°C , so that flue gas volume flow rate decreases, dust properties change, thereby enhancing the ESP performance [4].

2.1. Characteristics of LLTESP

LLTESP holds clear technological advantages over conventional ESP.

(1) Improvement on dust removal efficiency

After the temperature in an ESP is reduced, the flue gas volume flow rate is firstly reduced, resulting in a lower wind speed and longer residence time of aerosol particles in the electric field. Secondly, gas viscosity decreases, thus the drag resistance of air on the dust particles decreases. Moreover, as flue gas density increases, the operating voltage of ESP can also be raised. Meanwhile, the electrical resistivity of fly ash can usually be reduced to a suitable range. All these effects after lowering the temperature would be beneficial in improving the ESP efficiency. Therefore LLTESPs have a higher dust removal efficiency than

the conventional ESP, thereby emission reduction can be achieved in coal-fired power plants.

(2) Favoring SO₃ collection, suppressing low temperature corrosion

In conventional ESP, gaseous SO₃ is difficult to capture. SO₃ capture efficiency of the following limestone-gypsum wet desulfurization system is not high either, easily causing low-temperature corrosion of downstream pipe and chimney. In LLTESP, flue gas temperature has dropped below the acid dew point, so that most of SO₃ in flue gas condenses to form mist adhesion on the dust particles surface, which is collected together with the dust (i.e., SO₃ condensation has a conditioning role to dust collection), thus reducing the low-temperature corrosion of gas pipework and chimney.

(3) Remarkable energy saving, operating cost reduction of plant

In the case LLTESP, if the recovered waste heat is used for heating of boiler condensate, can save coal consumption, improving boiler efficiency. If the recovered waste heat is used for heating the flue gas after the wet desulfurization, the increase in flue gas temperature will reduce wet stack corrosion and visible plume. Lower flue gas temperature reduces cooling water consumption in the wet desulfurization process and related costs. Although adding heat exchanger will introduce some pressure drop, power consumption of fan remains essentially the same due to the decreased gas volume flow rate. Nevertheless, power consumption of the pressure boosting fan for wet desulfurization is reduced, and the related power costs can be reduced. Therefore, LLTESP can save energy, reduce plant operating costs.

2.2. Development of LLTESP

The first LLTESP, appeared in 1970s, was applied in Liddell power station Australia. This power plant was burning Australia Bayswater low sulphur coal, generating the fly ash of high resistivity. To solve the emission problem, power plant attempted to apply primary air preheaters and secondary air preheaters to reduce the flue gas temperature to around 90°C, then dust removal efficiency of ESP improved significantly. As a representative parameter of ESP performance, the migration velocity was increased by 70% than that at 160°C [2]. In 1980s, Denmark Ensted power plant modified the coal to a low sulphur one. To address the high resistivity fly ash problems, ESP working temperatures was reduced from 130°C to 105°C, drawing on the Liddell power station experience, together with the newly introduced Semi-pulse-Intermittent Energization. As the result, twice times more effective migration velocity of dust was achieved [5]. In the 90's, Japan developed LLTESPs, thereby air preheater was followed by a non-leakage GGH and flue gas temperature was reduced below 100°C. The dust concentration at the ESP exit could reach less than 5 mg/Nm³. Meanwhile, the recovered heat from GGH of flue gas was used for heating wet desulfurization, preventing

the wet stack and visible smoke plumes. Since then, LLTESP was received widespread applications in Japan [6].

2.3. Application of LLTESP in China

In recent years in China, with the rapid economic development, and the installed capacity of coal-fired power plants has been continually growing rapidly, which is becoming one of the important factors of large scale haze pollution. In order to improve the environment, the Chinese Government issued the "Emission standard of air pollutants for thermal power plants (GB 13223-2011)", which stipulates a dust emission concentration limit as 30 mg/Nm³ in general regions, 20 mg/Nm³ in key regions. The new standard has brought new challenges for ESP technology. In order to meet the requirements of the new emission standard, coal-fired power plants are required to seek new technical approaches to achieving ultra-low emission of dust. Successful experiences abroad show that LLTESP can achieve the double targets of both energy saving and emission reduction [7], which provides new thoughts for energy energy-saving and emission reduction in coal-fired power plant in China.

A number of successful cases of engineering implementation of LLTESPs in Datang Ningde Power plant #4 boiler-600 MW Unit, Jiangxi Xinchang Power Plant #1 Boiler-660 MW Unit, etc. have opened large scale applications of LLTESP in coal-fired power plants of China. Currently LLTESP has become an important flue gas control device to realize ultra-low emission in coal-fired power plants of China [8].

2.4. LLTESP Technology in Longking

Fujian Longking Co., Ltd. (Longking for short) is the largest environmental equipment supplier in China. In 2006, the company is the first in China to carry out research work of LLTESP. In 2010 a breakthrough prototype was made, and Longking's LLTESP new products (LSC LLTESP) were formed. In 2012, nationally the first 600 MW unit LLTESP was applied in Datang Ningde power plant's efficiency promoting renovation project, with all indexes having reached a better level.



Figure 1. Longking LLTESP exemplary project (Datang Ningde Power Plant 600MW Unit LLTESP)

The company has put LLTESP into operation with a cumulative 30 GW installed capacity, a global leader in terms of commercialization accomplishment.

2.5. Issues requiring investigation in LLTESP technology

Massive applications of LLTESPs in China pose a challenge for technology development. Engineers urgently need to understand dust removal mechanisms under such conditions, need to study and analyse the qualitative and quantitative relationship between performance and influential factors, including the following aspects:

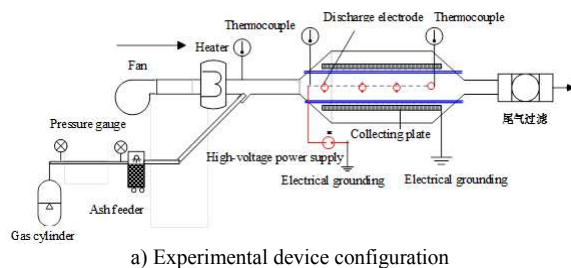
- Regarding the mechanism, apart from reducing dust resistivity in LLTESP, how are other factors affecting dust removal efficiency (such as the amount of charges, working voltage, SO₃ deposition, particulate coagulation) changing?
- For particles with different diameters, how is the dust removal efficiency affected? Especially what happens to the fine particles collection characteristic?
- Comparative tests of ESP performance improvement under different engineering conditions (coal type, operating condition), when the flue gas temperature is reduced.
- From a long-term perspective, gradually establish a mature computer model for the analysis of impact parameters and the prediction of performance. Our work in this area will be described below.

3. Experimental Study of LLTESP

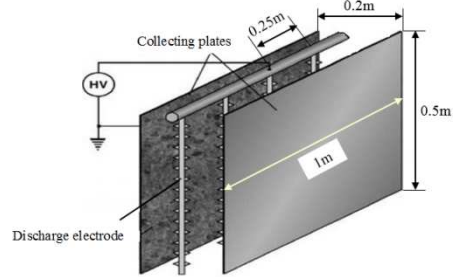
In order to elucidate LLTESP dust removal mechanism and influence factors, Longking, collaborating with Tsinghua University conducted experimental study in classification of LLTESP grading dust removal efficiency, dust charging, fine particulate capture, SO₃ removal etc. The factors influencing the performance of LLTESP are studied respectively under laboratory conditions and field conditions.

3.1. Effect of temperature on dust removal efficiency and charge amount under laboratory condition

For comparative analysis of the effect of various flue gas temperatures on the performance of ESPs, temperature controllable ESP test rig was established for the ESP process experiment. By changing the inlet temperature, the effect on dust removal efficiency and charge was studied. ESP test rig is shown in Figure 2. Air temperature can be heated up to 150°C, and flue gas pipe and ESP shell are thermally insulated, with temperature difference between the inlet and outlet of ESP guaranteed within 3°C. Dust powders after mixed with air flow into the ESP together.



b) Photo of experimental device



c) Dimensions of experimental ESP

Figure 2. Schematic ESP test rig

Lab ESP dimensions, gas velocity are selected in accordance with the principles of main governing equations of ESP in the process, to ensure a similar residence time in the test rig to practical ESP, a similar flow field and space charge distribution and electrical corona wind as the basic principles. Specific process is omitted here.

Table 1 lists the composition of the ash samples used in the experiments. Malvern laser particle size analyzer is used for the analysis of particle size distribution as shown in Figure 3.

Table 1. The composition of the ash samples used in experiment

Composition	Content(%)	Composition	Content(%)
Fe ₂ O ₃	6.55	K ₂ O	1.00
SiO ₂	51.11	CaO	4.87
Na ₂ O	0.42	Al ₂ O ₃	29.26
MgO	0.99	MnO ₂	0.06
TiO ₂	1.07	—	—

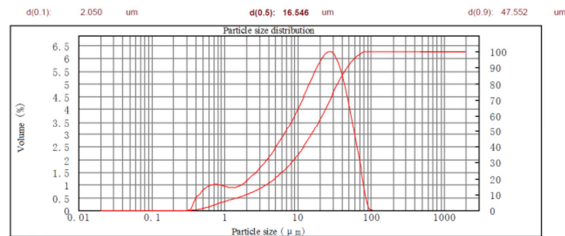


Figure 3. Ash sample particle size used in experiment

The electrical resistivity of test fly ashes is analysed off-line, and the results are shown in table 2 and Figure 4, where the blue and red lines represent the tested temperature of 90°C and 130°C respectively. The offline resistivity in low temperature stage increases as the temperature rises, peaking at 157°C, and then decrease with increasing temperature. Its value at 90°C is an order of magnitude smaller than at 130°C.

Table 2. Fly ash offline resistivity in relation to temperature

Temperature °C	80	105	120	130	157	185
Resistivity (Ω·cm)	3.16×10 ⁹	4.36×10 ¹⁰	8.44×10 ¹⁰	1.02×10 ¹¹	2.07×10 ¹¹	1.73×10 ¹¹

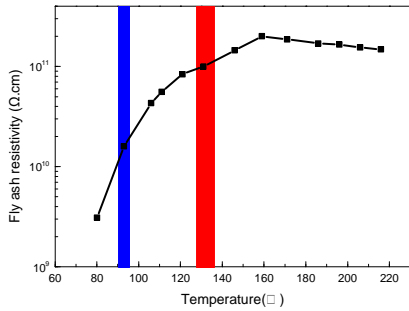
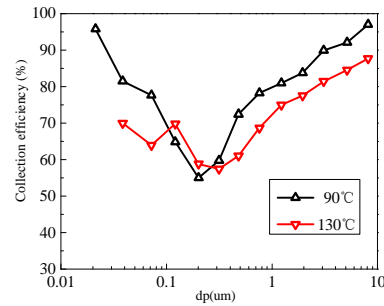


Figure 4. Offline resistivity of fly ash used in experiment

Electrical low pressure impactor (ELPI) is used to measure ESP entrance/exit dust concentration and the exiting charges. With working voltage of 20 kV and wind speed of 0.31 m/s, dust concentrations at ESP entrance/exit, removal efficiency and exiting charge for 90°C and 130°C are shown in Figure 5 and Figure 6.

Figure 5 shows at the temperatures of 90°C and 130°C, grading dust removal efficiency has a lowest value found within the interval 0.1-0.3 μm. Outside this interval, 90°C condition other particle removal efficiency is higher under 90°C than under 130°C.

Figure 6 shows, compared with 130°C, significant increase in the average quantity at 90°C, where the increase of charge on the particles smaller than 2.5 μm is particularly evident.



c) Comparison of dust grading efficiency for 90°C and 130°C
Figure 5. Effect of temperature on grading dust removal efficiency

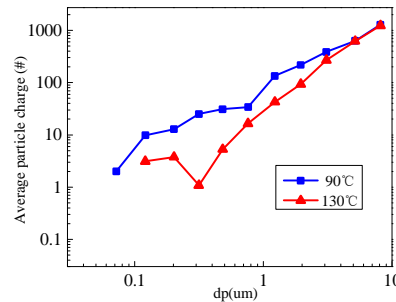
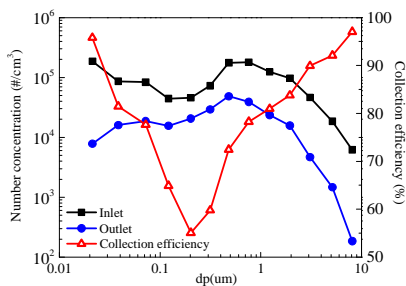
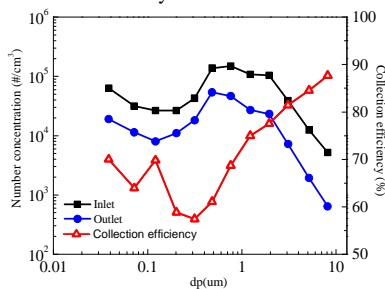


Figure 6. Effect of Temperature on outlet particle charges



a) ESP inlet/outlet dust concentration and grading removal efficiency for 90°C



b) ESP inlet/outlet dust concentration and grading removal efficiency for 130°C

3.2. Field measurement of commercial LLTESP

For a 300 MW unit, in order to meet emission requirements, the original ESP design is modified as a low-low temperature one, a heat exchanger is added right before the ESP to reduce the flue gas temperature. In this LLTESP, by changing the operation of the heat exchanger, flue gas temperature can be adjusted to 130°C, 93°C, 84°C as required. Under various temperature conditions, the dust resistivity, grading dust removal efficiency and exiting charges are measured online.

(1) Effect of temperature on online dust resistivity

Under offline conditions, the change of the flue gas conditions in contact with the dust layer makes it difficult for laboratory test to reflect the real dust resistivity under working conditions, so online measurement is necessary. Under different temperature operating conditions, on-site online test results of dust resistivity at the ESP entrance is given in table 2. Flue gas temperatures up to 130°C down to 93°C, 84°C, the online dust resistivity decreases as temperature decreases.

Table 2. Dust online resistivity under different temperatures

Temperature (°C)	Applied voltage (V)	Resistivity (Ω·cm)
130	100, 250, 500, 1000	6.09×10 ¹¹
93	100, 250, 500, 1000	2.46×10 ¹¹
84	100, 250, 500, 1000	1.60×10 ¹¹

(2) Effect of temperature on grading dust removal efficiency

Using ELPI, the number concentrations of dust particles at the inlet and outlet of ESP varying with particle size are measured under different temperature conditions. The corresponding grading dust removal efficiency is calculated, with results shown in Figure 7.

Under the same temperature working conditions, the removal efficiency close to 0.1 μm is lower compared with other particle size range. As the size increases, overall classification efficiency tends to increase, particularly for particle size greater than 1 μm, dust removal efficiency increases evidently.

A comparison of grading dust removal efficiency under various temperatures indicates that, with decreasing flue gas temperature, dust removal efficiency increases. At the gas temperature of 84°C, dust removal performance in the entire particle size range is higher than at 130°C and 93°C.

(3) Effect of temperature on PM10, PM2.5 mass removal efficiency

ELPI gives ESP inlet and outlet dust concentration distribution in terms of particle numbers. The inlet and outlet grading concentration in mass can be calculated according to equation (1):

$$M_i = \frac{\pi}{6} (Di)_i^3 \rho N_i \quad (1)$$

where i is stage number; ρ is dust density (2600 kg/m³), Di is geometric mean diameter of stage i .

Mass removal efficiency for PM10 and PM2.5 is calculated from eq (2).

$$\eta = (1 - m_{\text{outlet},j} / m_{\text{inlet},j}) \times 100\% \quad (2)$$

Where $m_{\text{inlet},j}$, $m_{\text{outlet},j}$ are mass concentrations of PM10 or PM2.5 at the inlet and outlet of ESP respectively.

Under different temperature conditions, ESP inlet and outlet PM10, PM2.5 mass concentration and removal efficiency are listed in Table 3.

It can be seen that with the decreasing flue gas temperature, removal efficiency for both PM10 and PM2.5 is improved, notably the removal efficiency of PM2.5 is remarkable.

The removal efficiency of PM10 and PM2.5 is transformed to their penetration rate (1 - η), as shown in Figure 8. As can be seen from the figure, after the flue gas temperature drops, PM10 and PM2.5 penetration rates are significantly reduced, suggesting that LLTESP have a significant technical advantage over conventional ESP for removal of fine particles.

Table 3. Mass concentration and removal efficiency of PM10 and PM2.5 for different temperatures

Temperature (°C)	PM10 mass concentration (mg/Nm ³)		PM10 removal efficiency (%)	PM2.5 mass concentration (mg/Nm ³)		PM2.5 removal efficiency (%)
	Inlet	Outlet		Inlet	Outlet	
130	904.4	29.4	96.7%	276	11.3	95.9%
93	632.1	12.3	98.0%	225.4	5.5	97.5%
84	645.3	11.9	98.2%	224.5	4.5	98.0%

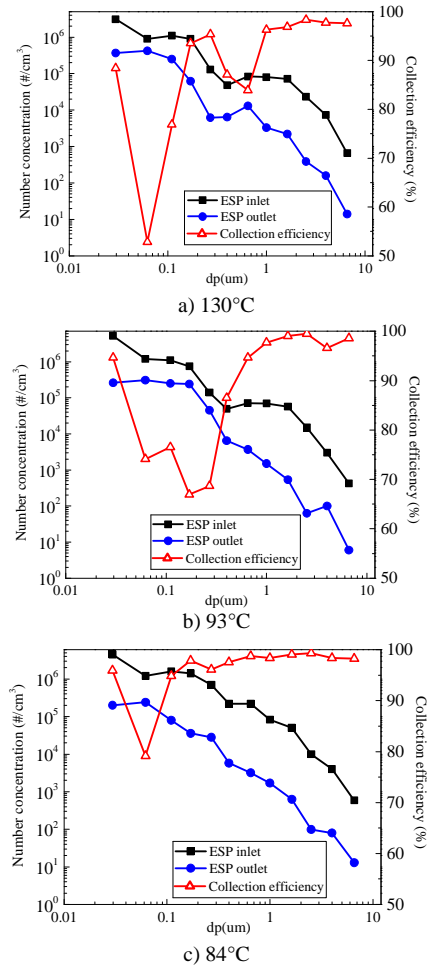


Figure 7. Effect of temperature on grading dust removal efficiency

(4) Effect of temperature on particle charge

Under different temperatures, dust particle charges and charging ratio (of the actual charge and saturation charge) at the ESP outlet are shown in Figure 9. At the same temperature, the charge increases with increasing particle size, but over the particle size range, charged particles are difficult to achieve saturation. The general trend of the results is, the average charges on the dust particles get promoted as flue gas temperature is reduced.

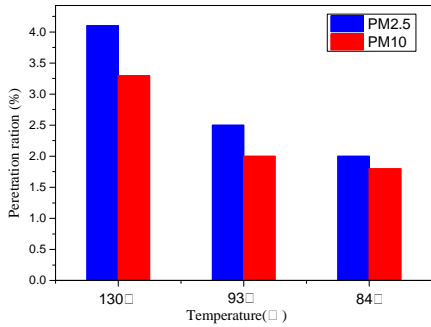
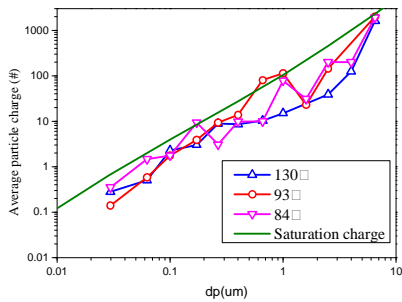
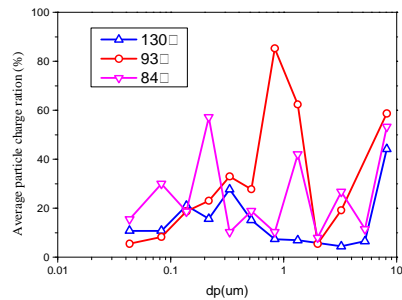


Figure 8. Penetration rate of PM10 and PM2.5 under different temperatures



a) Particle charges at different temperatures



b) Particle charging ratio at different temperatures

Figure 9. Effect of temperature on particle charge

(5) Comparison of field tests of LLTESP

To obtain the information on the dust removal performance of LLTESP under different kinds of coal, operating conditions, Longking measured the dust removal efficiency of a number of power plant LLTESPs under different temperatures. Four power plant test results are shown in Table 4.

Table 4. A list of dust removal efficiency of different power plant LLTESP

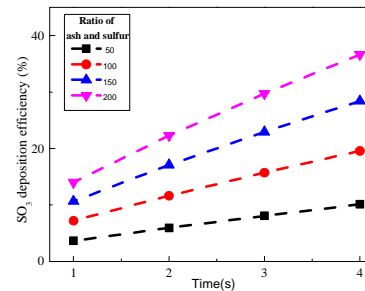
	Temperature °C	Inlet concentration mg/Nm ³	Outlet concentration mg/Nm ³	Collection efficiency %
No.1 power plant 600MW unit LLTESP	120	7895	90.6	98.852
No.2 power plant 660MW unit LLTESP	97	7860	29.3	99.627
No.3 power plant 135MW unit LLTESP	147	40021	42.6	99.894
No.4 power plant 135MW unit LLTESP	103	39820	13.1	99.967
No.5 power plant 135MW unit LLTESP	154	2275	15.2	99.332
No.6 power plant 135MW unit LLTESP	122	2102	9.8	99.534
No.7 power plant 135MW unit LLTESP	148	23760	98.2	99.558
No.8 power plant 135MW unit LLTESP	117	20300	16.3	99.918

unit LLTESP

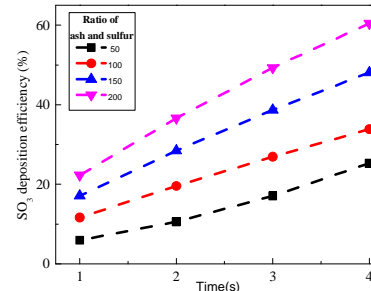
After the accumulated engineering test results are summarized and analysed, one will learn about the performance boosting coefficient of LLTESP under different kinds of coal and different working conditions, which can be used as selection guidance of new LLTESP designs (including modification).

(6) Effect of ash-sulphur ratio, SO₃ concentration on SO₃ deposition

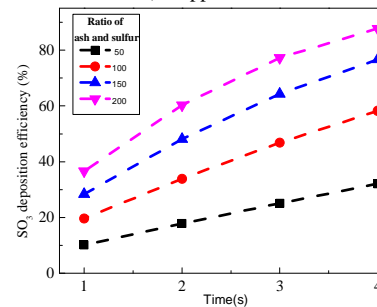
To study the factors affecting the dust deposition rate of SO₃ in LLTESP, we developed a theoretical model of sulfuric acid droplets-particles aggregation. For different SO₃ content in the flue gas, ash-sulfur ratios, SO₃ deposition scenario calculated is shown in Figure 10.



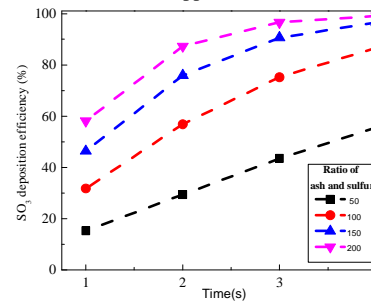
a) 5 ppm SO₃



b) 10 ppm SO₃



c) 20 ppm SO₃



d) 40 ppm SO₃

Figure 10. Effect of ash-sulphur ratio on deposition rate for different SO₃ content

The results indicate that SO_3 deposition rate increases with time, and ash-sulfur ratios and SO_3 concentration have a significant impact on SO_3 deposition. Under the same SO_3 content, as ash-sulfur ratios increase, the deposition rate of SO_3 increases. Take a SO_3 content of 10ppm for example, ash-sulfur ratio of 50, then maximum deposition rate of SO_3 is 20%. When the ash-sulfur ratio is increased to 200, SO_3 maximum deposition rate will be raised to 60%. In addition, under the same ash-sulfur ratio, when SO_3 content increases, the SO_3 deposition rate is also increased.

4. Numerical modelling of LLTESP

ESP is a complex physical process. In recent decades, world-wide researchers have made a lot of progress in the theoretical aspects on electric field, particle charging, dust-gas flow, dust deposition, etc. On the whole, however, we have not been able to fully understand ESP process theoretically. Many studies still rely on experiment testing and on-site debugging. Therefore the study of ESP as a whole is far from enough. In parallel with experimental and theoretical research, numerical simulation can deepen the theoretical analysis on the one hand, on the other hand can generate data that cannot be obtained experimentally, so as to explore the nature of specific phenomena of ESP.

4.1. A short historical review of numerical modeling of ESP

With the development of numerical computing, numerical simulation technology has been applied to the ESP study. In 1970's, numerical methods first began to be applied to solve electric field Poisson equation and current continuity equation. Yabiet al. [9], Yamaoto and Velkoff [10], Ushimaru and Butler [11] used finite difference method to solve the above governing equations, but their model needs surface current density and the applied voltage to determine current density boundary conditions on the corona wire. Later, McDonald, Smith and Spence [12] also used the finite difference method in wire-plate ESP control equation. Sekar and Stomberg [13] used orthogonal transform method to simulate the electric distribution in a plate type ESP. Kallio and Stock [14] numerically calculated electric field and space charge distribution in a wire-plate type ESP using a hybrid method (finite element near the corona wire, while finite difference far from the wire).

With the advancing computing capabilities, numerical simulation technologies are increasingly being used to predicting inner flow field of ESP. In numerical simulation of airflow distribution, Nielsen et al. [15] considered ESP components such as flow distributor. The simulation results are compared with experimental tests, pointing out that the numerical simulation technology of internal airflow in ESP is an effective detection tool, and can replace experiment tests, shortening test time of air distribution. Veronique Ar-

rondeli et al. [16] used Fluent and N3S software to calculate three dimensional airflow distribution in ESP, with a scope including inlet pipelines, inlet diffuser, inside electric field, outlet trumpet. Horizontal velocity components of air flow were presented respectively at inlet/outlet cross section, which were consistent with test results. Canada's Arthur G. Hein used two dimensional CFD model of ESP to study a skew gas-flow technology. The results show that CFD numerical simulation is helpful in optimization of smoke movement and air flow, can successfully predict performance improvement of dust collector with the skew airflow technology [17].

An overview of the past, although numerical simulation technology of ESP has been developed, most studies were in favour of numerical simulations of a specific process phenomenon: electric field, airflow, electrohydrodynamic, while numerical simulation study of ESP system performance is lacking.

4.2. Main methodology and innovation of present study

Longking and University of New South Wales started a collaborative project from 2007 in numerical simulation of ESP. Models of air flow, electric field, gas-particle two phase flow, integrated ESP were developed, which provided new technical support to the study of LLTESP.

The main method of the present study [18-22] is to establish mathematical model for electrostatic precipitation process. Finite volume method is used to solve a variety of transport equations to achieve quantitative calculations of physical quantities in the ESP process. Compared with many other numerical simulations of ESP, innovations of this research are:

- (1) Proposed a method of multi-scale CFD simulation of airflow distribution of ESP and tackled the modeling difficulty of ESP micro-scale flows, such as perforated plates, groove boards, etc.
- (2) Numerical simulation study is more systematic, comprehensive, covering several submodels such as gas flow, electric field gas-particle flow and so on, and an integrated model.
- (3) Effects of such factors as geometry, temperature, acid adsorption, particle charging, back corona, on ESP collection efficiency are considered systematically.

4.3. Contents and results of numerical modelling of LLTESP

- (1) Numerical modelling of gas flow distribution

Gas flow distribution is so important that its uniformity will make 20%~30% difference in ESP efficiency. A difficulty in the numerical simulation of gas flow distribution is smoothing perforated plate and grave board, because they have either too many holes or structures of small size, which are difficult to mesh. Engineers generally set the parameters based on past experience of orifice and groove boards, thus lack of reliability. A multiscale method is presented in this

paper, thereby flow distribution in ESP is simulated at micro-scale, medium-scale and large scale respectively (Figure 11). At micro-scale, unit cell model is established for perforated plate and grave board, numerical simulation of gas flow within micro-hole determines the resistance coefficient of the perforated plate and grave board. At medium scale, the parameters obtained above for perforated plate and grave board are used to simulate flow characteristics and parameters of a single ESP body unit. At the large scale, the ESP unit parameters obtained at the medium scale are used to simulate the flow in the entire ESP network system.

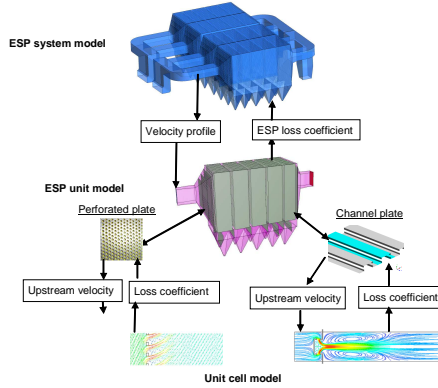


Figure 11. Multiscale CFD method for the gas flow in an ESP system

In the numerical simulation of gas flow distribution, assuming Newtonian incompressible gas, flue gas flow in steady-state follows the equation of conservation of mass and conservation of momentum equation:

$$\nabla \cdot (\rho_f \mathbf{U}) = 0 \quad (3)$$

$$\nabla \cdot (\rho_f \mathbf{U} \otimes \mathbf{U}) = \nabla \cdot (p + \frac{2}{3} \rho_f k) + \nabla \cdot [(\mu + \mu_t)(\nabla \mathbf{U} + (\nabla \mathbf{U})^T)] \quad (4)$$

ρ_f is flue gas density, kg/m^3 ; \mathbf{U} velocity, m/s ; P pressure, Pa ; k turbulence kinetic energy, m^2/s^2 ; μ dynamic viscosity, $\text{N}\cdot\text{s}/\text{m}^2$; μ_t turbulent viscosity, $\text{N}\cdot\text{s}/\text{m}^2$.

In addition, the two equation k - ε turbulence model is chosen.

The numerical simulation results of gas flow distribution in a 1000 MW unit LLTESP are shown in Figure 12, measures are taken (installing/adjusting in-pipe baffles, perforated plates and guide vanes), to optimize the flow field, making the deviation of flow rate to each pass within 5%, root-mean-square speed before the electric field less than 0.2. The mean velocity in each pipe is compared between numerical simulation and physical test result, with deviation in 3%.

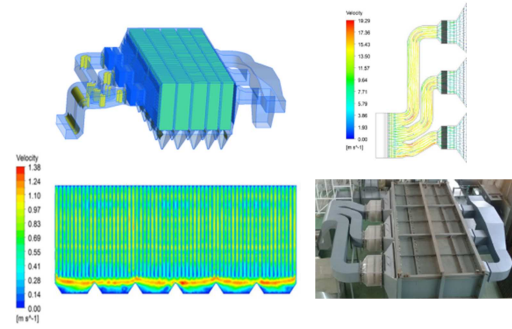


Figure 12. A 1000 MW Unit ESP gas flow simulation and experimental rig

(2) Numerical modelling of electric field distribution

When ESP is powered, the electric field is established between corona wires and collection electrodes, providing driving force to dust separation from flue gas. Electric field distribution is a main factor determining ESP performance, affecting corona generation, charging and migration of particles in electric field.

The fundamental governing equations to describe the electric field-Poisson equation and current continuity equation:

$$\nabla^2 V = -\rho_{\text{ion}} / \varepsilon_0 \quad (5)$$

$$\nabla \cdot (\rho_{\text{ion}} b \mathbf{E}) = 0 \quad (6)$$

$$\mathbf{E} = -\nabla V \quad (7)$$

$$\mathbf{J} = b \rho_{\text{ion}} \mathbf{E} \quad (8)$$

where V is electrical potential, V ; ρ_{ion} space charge density, C/m^3 ; ε_0 permittivity, F/m ; b ionic mobility, $\text{m}^2/(\text{s}\cdot\text{V})$, related to temperature and gas composition; \mathbf{E} field intensity, V/m ; \mathbf{J} current density, A/m^2 .

According to Lawless and Sparks, ionic mobility depends on temperature as eq (9) [23]:

$$b(T) = b_0 (T / 273.16)^\beta \quad (9)$$

where b_0 and β are evaluated by fitting the experimental data [21]:

$$b_0 = 2.092 \times 10^{-4} \exp\left(-\left(\frac{mf_{\text{H}_2\text{O}}}{16.59}\right)^{0.261}\right) \quad (10)$$

$$\beta = 1.43 + \ln\left(1 + \left(\frac{mf_{\text{H}_2\text{O}}}{1.1425}\right)^{0.6}\right) \quad (11)$$

T is gas temperature, K ; $mf_{\text{H}_2\text{O}}$ water mass fraction.

Peek equation is used to determine the corona onset field [24]:

$$E_0 = 2.7 \times 10^6 [V \cdot \text{m}^{-1}] \delta m \left(1 + \frac{0.054 [m^{0.5}]}{\sqrt{\delta r}}\right) \quad (12)$$

$$\delta = \frac{PT_0}{P_0T} \quad (13)$$

E_0 is corona onset field, V/m; δ relative density, i.e., the ratio of actual gas density and the density of normal state; T_0 represents normal temperature, 273K; P_0 normal atmospheric pressure, 101325 Pa; r , corona wire radius of curvature; m , pollution coefficient.

For clear collection plate without dust layers, maximum working voltage depends on the electric field breakdown voltage of ESP. When the maximum field strength at the collection plate reaches its corona onset threshold, the electric field is considered as breakdown [21]. The radius of curvature of the collection plate $r = \infty$. Under standard atmospheric pressure, according to Eqs (12) and (13), the corona onset field is derived as:

$$E_{0(r=\infty)} = \left(\frac{T_0}{T}\right) 2.72 \times 10^6 [V/m] \quad (14)$$

Ion charge density on the corona electrode:

$$\rho_0 = ab\epsilon_0 E_0 (E - E_0), E \geq E_0 \quad (15)$$

a is an empirical constant, $0.05 \text{ s}^2/\text{m}^2$ [20].

Taking the wire-plate ESP single channel structure (Figure 13) as an example, we simulated the electric field in ESP with configuration: corona wire diameter 3.5 mm, wire-to-wire spacing 200 mm, plate-to-plate distance 400 mm. Electric boundary conditions: 0 kV at collection plates, a given input voltage (negative) applied at corona wire. Simulations are undertaken in the framework of ANSYS CFX software. By changing temperature, simulation results of electric characteristics can be obtained for different temperatures (90°C, 120°C, 150°C). Figure 14 shows simulated electric field for 90°C: a corona zone of high field strength forms in a close space around the wire. The field strength gradually decreases towards the dust collection plate.

Calculated breakdown voltages under different temperatures are shown in table 5. When temperature drops from 150°C down to 90°C, the breakdown voltage rises from 72.8 kV to 85 kV, close to the experimental results. In the experiment, electrodes with a layout shown in Figure 13, are placed in the heating cabinet, and when heated to the desired temperature, electric breakdown voltage is measured. Therefore, numerical simulation results indicate that when temperature decreases, the ESP allows a higher operating voltage.

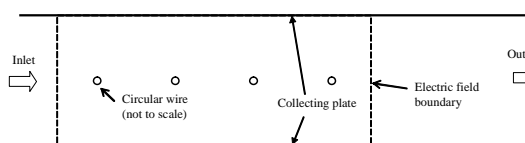


Figure 13. Wire-plate type single channel ESP model

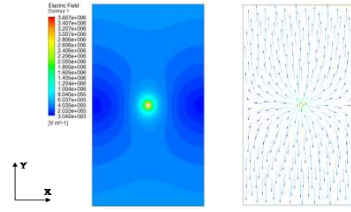


Figure 14. Simulated electric field at 90 °C

Table 5. Breakdown voltage-comparison between experiment and simulation ($m = 0.25$)

Gas temperature(°C)		90	120	150
3.5mm smooth wire	Experiment(kV)	94.3	86.5	77.5
	Simulation(kV)	85.0	78.4	72.8
Barbed wire (needle pointing plate)	Experiment(kV)	82.0	70.6	63.8
	Simulation(kV)	85.6	78.8	73.1
Barbed wire (needle parallel to plate)	Experiment(kV)	84.0	71.3	69.5
	Simulation(kV)	91.8	84.7	78.4

The round corona wires are replaced by needled wires, with electrodes' spacing remained the same. Three-dimensional electric field are numerically simulated for two cases, i.e., needles perpendicular to the plate and needles parallel to the plate respectively. Common in both cases, the electric breakdown voltage increases with decreasing temperature. Under the same temperature, the breakdown voltage is higher in the case of needles parallel to the plate than the other case, which is consistent with the experimental results, as shown in Table 4. Besides, the needle orientation has an impact on current density distribution of dust collection plate. In the case of needles parallel to the plate, the current density is more uniform, with different patterns shown in Figure 15. Due to the higher breakdown voltage and more uniform current density, the configuration with needles parallel to the collection plate can be selected in practical LLTESP.

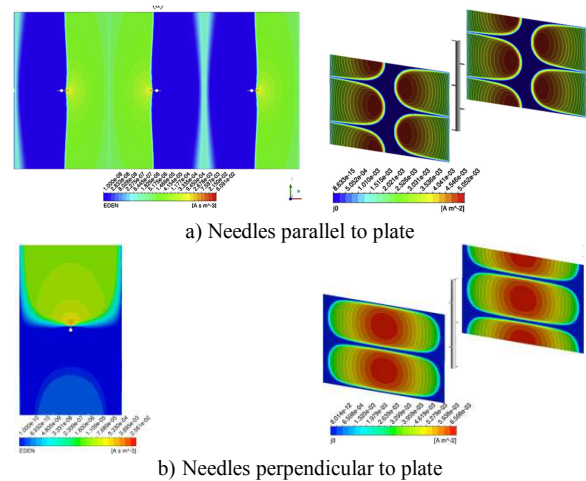


Figure 15. Simulated electric field for needled corona wire

(3) Simulation of particle charging and motion
Particle charging rate is calculated using Lawless model [25]:

$$\frac{dv}{d\tau_q} = \begin{cases} f(w) \frac{v-3w}{\exp(v-3w)-1}, & v > 3w \\ \frac{3w}{4} \left(1 - \frac{v}{3w}\right)^2 + f(w), & -3w \leq v \leq 3w \\ -v + f(w) \frac{-v-3w}{\exp(-v-3w)-1}, & v < -3w \end{cases} \quad (16)$$

$$v = \frac{qq_e}{2\pi\epsilon_0 d_p k_0 T}, \quad w = \frac{\kappa_p}{\kappa_p + 2} \frac{Ed_p q_e}{2k_0 T}, \quad \tau_q = \frac{b\rho_{ion} t}{\epsilon_0},$$

$$f(w) = \begin{cases} (w+0.475)^{-0.575}, & w \geq 0.525 \\ 1, & w < 0.525 \end{cases}$$

q_e is unit ion charge, C; κ_p is dielectric constant of particle.

Particle dielectric constant:

$$\kappa_p^{1/3} = \sum_{i=1}^n v_i \kappa_i^{1/3} \quad (17)$$

κ_i dielectric constant of component i , v_i mass fraction of component i . The dielectric constant of the fly ash in Table 1 is calculated to be 6.6.

Equation of particle motion:

$$m_p \frac{d\mathbf{u}_p}{dt} = \frac{1}{8} C_D \pi d_p^2 \rho_f |\mathbf{u}_f - \mathbf{u}_p| (\mathbf{u}_f - \mathbf{u}_p) + \frac{1}{6} \pi d_p^3 \mathbf{g} (\rho_p - \rho_f) + q\mathbf{E} + \mathbf{F}_{dis} \quad (18)$$

$$C_D = \frac{24}{C_C Re_p} (1 + 0.15 Re_p^{0.687}) \quad (19)$$

m_p is particle mass, kg; \mathbf{u}_p particle velocity, m/s; \mathbf{u}_f gas velocity, m/s; d_p particle diameter, m; ρ_p particle density, kg/m³; ρ_f gas density, kg/m³; q particle charge, C; \mathbf{F}_{dis} dispersion force, N; Re_p Reynolds number. C_C is Cunning correction factor, which can be calculated as [26]:

$$C_C = 1 + \frac{2\lambda}{d_p} (1.257 + 0.4 \exp(-\frac{1.1d_p}{2\lambda})) \quad (20)$$

Free pass of molecules:

$$\lambda = \frac{k_B T}{\sqrt{2} \pi d_{mol}^2 P} \quad (21)$$

k_B Boltzmann constant, J/K; d_{mol} diameter of molecule, m.

According to the flue gas temperature and pressure in ESP, the flue gas is taken as ideal gas. The flue gas density obeys the equation of state of ideal gases (11). The kinetic theory of molecules is used for gas dynamic viscosity in relation with temperature [27].

Ash-entrained gas passes the electric field at 1 Nm/s and exit the ESP through the outlet, the coupled gas flow, particle charging, particle flow are

solved numerically, and particle trajectories of different size 0.05–25 μm are obtained (Figure 16).

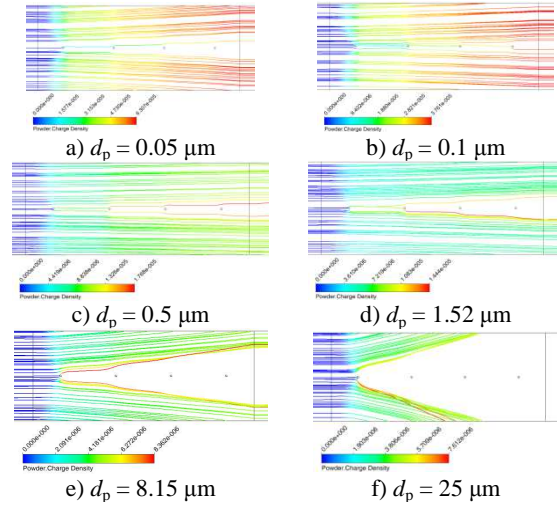


Figure 16. Particle trajectories for different particle sizes

As can be seen from Figure 16, particle surface charge density reaches its maximum near the corona region where is most favorable to particle charging. Large particles are captured by the collection plate under electrical force, before saturation charges were reached, thus their surface charge density is small. Small particles stay longer, thus continuously charging for longer time. As the particle size decreases, diffusion charging plays more and more important role, so that small particles can absorb more charges without restrictions. Therefore, with decreasing particle size, particle surface charge density is increased. Particle collection efficiency is related to particle trajectories. If a particle trajectory is able to reach the plate, this particle can be collected. Figure 16 displays particles diameter $d_p = 0.5 \mu\text{m}$, few particles trajectories can arrive at the plate, suggesting lowest dust removal efficiency. When particles diameter is less than $0.5 \mu\text{m}$, due to increasing diffusion charging and reduced gas drag force (particles diameter and gas molecular average free pass are getting close), dust removal efficiency improves. When particles diameter is greater than $0.5 \mu\text{m}$, particles removal efficiency increases with increasing diameter.

(4) Effect of dust resistivity

Dust particle resistivity is closely related to temperature, and affected by dust composition, moisture of flue gas, etc. Bickelhaupt [28] obtained resistivity correlations, where volume resistivity in Ohm-m is:

$$\rho_v = \exp(3.62876 - 1.8916 \ln X - 0.9696 \ln Y + 1.237 \ln Z - 0.069078 \times 10^{-5} E + 9980.58/T) \quad (22)$$

Surface resistivity in Ohm-m is:

$$\rho_s = \exp\left(\frac{27.59774 - 2.233348 \ln X - 0.00176W - 0.069078 \cdot 10^{-5} E - 0.00073895W \exp(2303.3/T)}{T}\right) \quad (23)$$

The combined dust resistivity is:

$$\frac{1}{\rho_d} = \frac{1}{\rho_v} + \frac{1}{\rho_s} \quad (24)$$

X is the atom concentration of Li and Na; Y is the atom concentration of Fe; Z atom concentration of Mg and Ca.

Based on the Bickelhaupt correlation, dust resistivity for the ash sample in Table 1 is obtained under different moistures and temperatures (Table 6).

Table 6. Calculated fly ash resistivity (Ωm)

Temperature (°C)	Water content (%vol)		
	0	5	9
90	6.886×10^{10}	8.380×10^9	1.546×10^9
120	6.480×10^{10}	1.846×10^{10}	8.926×10^9
150	4.838×10^{10}	2.472×10^{10}	1.342×10^{10}

Seen from Eqs (22) and (23), dust volume resistivity is affected by temperature and humidity-independent, whereas the surface resistivity is affected by both. In dry flue gas (zero moisture), dust resistivity decreases with increasing temperature (Table 6). Therefore, for a dry flue gas, temperature reduction increases the dust resistivity, undesired for dust removal. However, the actual boiler flue gases contain water. Under moist condition, when flue gas temperature is reduced from 150°C to 90°C, dust resistivity decreases with temperature. In addition, it can be seen from Table 5, under the same temperature, the higher the moisture, the smaller the dust resistivity, so water in the flue gas is beneficial to reduce the dust resistivity.

When a dust layer forms on the collection plate, maximum working voltage of ESP is limited by both electric field breakdown and back corona. Formation of dust layer on collection plates will create a voltage drop, causing an effective voltage loss:

$$\Delta V = J_d \rho_d d \quad (25)$$

J_d dust layer current density, same value as the current density at the collection plate, A/m^2 ; d dust layer thickness, m.

Field intensity in the dust layer:

$$E_d = J_d \rho_d \quad (26)$$

Whether or not back corona occurs depends on the maximum field intensity in the dust layer, E_{d-max} . When the electric field has not yet broken down, but the maximum field intensity in the dust layer E_{d-max} has already exceeded the dielectric strength, E_b , back corona will occur. When the electric field broke down, but E_{d-max} has not reached E_b , back corona cannot form. Therefore, the condition for back corona to occur is:

$$E_{p-max} < E_{0(r=\infty)} \quad (27)$$

$$E_{d-max} \geq E_b \quad (28)$$

E_{p-max} is maximum field intensity on the collection

plate, V/m ; E_{d-max} maximum field intensity in the dust layer, V/m ; E_b dielectric strength of dust layer, 2.2×10^5 [29] $\sim 1.8 \times 10^6$ V/m [30]. $E_b = 1. \times 10^6$ V/m in present study. Table 6 gives the dust resistivity calculated for dust layer thickness $d = 5$ mm, moisture content of 9%.

Numerical simulations of electric field give V-I characteristics under different flue gas temperatures with and without dust layer on the collection plate in Figure 17, where solid line denotes the case with dust layer, dotted line represents no dust layer on the collection plate. Without dust layer on the plate, V_a is the voltage difference between corona and collection plate. When a dust layer forms, V_a is the effective voltage drop between corona wire and the layer surface, i.e., the dust layer voltage drop is deducted from electrode voltage. J is the average current density on the collection plate.

Figure 17 shows: without dust layer, for the temperature of 150°C, and 120°C and 90°C, the maximum effective voltages are 72.8 kV, 78.4 kV and 85 kV respectively. With a dust layer, the corresponding maximum effective voltages become 25 kV, 34 kV and 66.8 kV respectively, suggesting that existence of dust layer makes the effective voltage reduced. At 90°C, the effective voltage is reduced to a less extent than at 150°C and 120°C, because dust resistivity decreases as temperature decreases, cause smaller voltage drop across the dust layer. Compared with the case of no dust layer, the dust layer allows smaller operating voltage range. If this range is exceeded, the dust layer maximum field intensity will exceed the dielectric strength, thus back corona will occur in ESP.

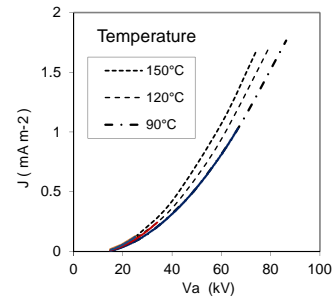


Figure 17. Simulated V-I curves with and without dust layer: dashed lines, no dust layer; solid lines, with dust layer

Figure 18 shows numerically simulated space-charge distribution at different temperatures and with dust layer. As temperature decreases, the effective voltage can be increased, thus the electric charge density at 90°C is greater than at 150°C and 120°C.

In addition, particle collection efficiency of different size particles predicted is shown in Figure 19. In the full size range considered, particle removal efficiency appears as "U" shape, with minimum efficiency between 0.2–0.5 μm . Collection efficiency of particles smaller than 0.2 μm or greater than 0.5 μm increases. When there is a dust layer, by resistivity, temperature has important implications for the effec-

tive voltage of ESP, which further affects particle collection efficiency. When temperature is reduced from 150°C to 90°C, the collection efficiency of dust particles of all different sizes has been significantly improved.

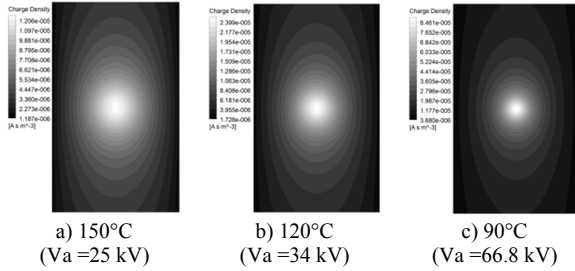


Figure 18. Simulated space charge density for the case with dust layer

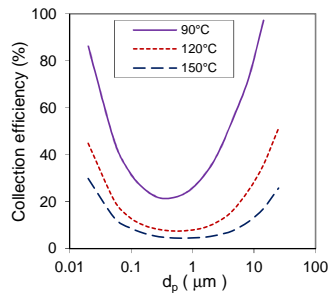


Figure 19. Simulated particle collection efficiency for different particle sizes with dust layer

(5) Numerical study on effect of acid condensation on ESP

Typically LLTESP operates at a temperature around 90°C. When the flue gas temperature falls below the acid dew point, gaseous SO₃ molecules combine with water vapor and condense to form liquid droplets of sulfuric acid. Due to high concentration of dust mass in the flue gas before LLTESP, particle specific surfaces is also high, thus acid mists easily adhere to dust particles surface. SO₃ mist adhesion on the dust particles surfaces are removed along with dust particles by LLTESP. SO₃ condensation and adhesion to dust particles play a role to reduce dust resistivity and facilitate particle coagulation [31-33], but the impacts of SO₃ condensation on particle charging were not studied. By numerical simulation, the present paper analyzed the impact of SO₃ condensation on dust collection efficiency via a change in dielectric constant.

Several correlations (Verhoff and Banchemo [34], Akkes [35], Pierce [36]) are exclusively for the prediction of the SO₃ dew point temperature. We used a new method to predict SO₃ acid dew point- Acid dew-point thermodynamic model. The partial pressure data of aqueous solution of sulfuric acid in Perry Manual [37] for water, SO₃ and H₂SO₄ in relation to temperature are fitted by an equation with coefficients dependent on the acid mass fraction. Based on mass conservation and phasic equilibrium, dew point can be calculated iteratively. Similarly, the amount and concentration of acid condensate can also be calculated under different

gas conditions. For different moistures, the acid dew point and acid concentration as a function of SO₃ concentration are shown in Figure 20. Acid dew point increases as SO₃ concentration increases. Moisture content affects the acid dew point, the greater the moisture content, the higher the acid dew point. Acid concentrations in the condensate increases with SO₃ concentration. Moisture content also affects sulfuric acid concentration, the greater the moisture content, the lower the concentration of sulfuric acid.

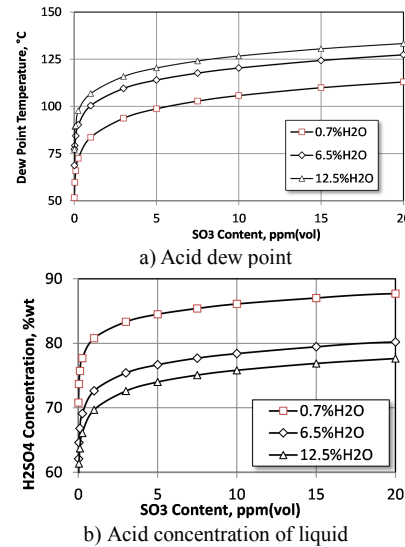


Figure 20. SO₃ condensation thermodynamic model result

Moisture content 9%(vol), dust concentration 10 g/Nm³ and SO₃ concentration 10 ppm are taken as base case conditions, and Figure 21 shows the quantity of condensate varying with temperature. Temperature has an important effect on condensation. Here the acid dew point of the base case is 123°C, water dew point is 44°C. When the temperature is lowered from the acid dew point, the quantity of acid condensate increases rapidly, relatively stable for 70°C ~100°C, and increases dramatically when close to water dew point.

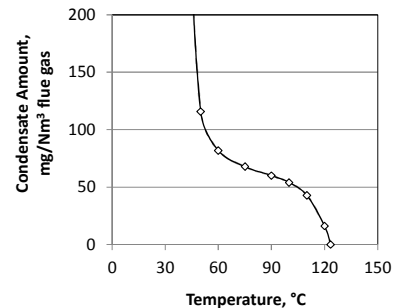


Figure 21. Quantity of condensate versus temperature

For a homogeneous particle, the saturation charge in an external electric field E_0 :

$$q_s = \frac{3\kappa_p}{\kappa_p + 2} \pi d_p^2 \epsilon_0 E_0 \quad (29)$$

Surface charge density is proportional to pe ,

$$pe = \frac{3\kappa_p}{\kappa_p + 2} \quad (30)$$

For a composite particle of two materials as sketched in Figure 22, κ_p in Eqs (29) and (30) is replaced by κ_{eff} [43]

$$\kappa_{eff} = \kappa_m \left(1 + \frac{3f\beta}{1-f\beta} \right) \quad (31)$$

$$\beta = \frac{\varepsilon_c - \varepsilon_m}{\varepsilon_c + 2\varepsilon_m} \quad (32)$$

$$f = (r_c/r_m)^3 \quad (33)$$

f is volume fraction.

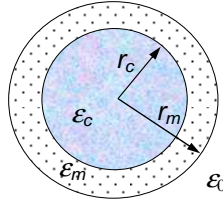


Figure 22. Composite particle

When acid mist adheres to the dust particle surface, a wet particle forms with the dust particle as core and the acid film as the shell. Since the dielectric constant of the acid is 80~100, far greater than that of dust particles (6~8), the particle after acid adhesion, according to Eq (31), has effectively increased its dielectric constant, apart from increased diameter. According to Eq (29), the wet particle will be able to acquire more charges than the dry particle.

When dust particles dielectric constant increases from 3.9 to 6.6, theoretically particle saturation charge can increase by 16%. Change in effective dielectric constant will lead to change in collection efficiency of different size particles. Numerical simulation results are shown in Figure 23. When the dielectric constant increases, the collection efficiency for particles greater than 0.1 μm particle is improved, but particles less than 0.1 μm are not affected. Compared with Figure 19, overall, the effect of acid condensation on aerosol particle charging limit, and subsequently on dust removal efficiency, is insignificant compared with the role of dust layer resistivity.

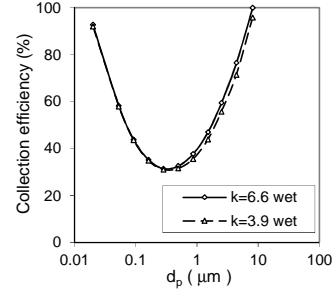


Figure 23. Effect of dielectric constant on dust removal efficiency

In addition to increasing particle effective dielectric constant, acid condensation affects dust resistivity. According to Bickelhaupt model, when SO_3 is present in the gas, acid resistivity should be considered:

$$\rho_a = \exp\left(\frac{54.324 - 0.85472 C_{\text{SO}_3} - 0.069078 \times 10^{-5} E - 13049.44 [K]/T}{1} \right) \quad (34)$$

C_{SO_3} is SO_3 concentration, ppm.

Combined resistivity is:

$$\frac{1}{\rho_{total}} = \frac{1}{\rho_v} + \frac{1}{\rho_s} + \frac{1}{\rho_a} \quad (35)$$

For the ash sample in Table 1, with SO_3 content of 10 ppm, resistivity values calculated are listed in Table 7. The results show that, the acid resistivity is 2~5 orders of magnitude smaller than the surface and volume resistivity, causing the dust resistivity to fall sharply. When SO_3 condenses, dust resistivity becomes so small that the voltage drop at the layer can be ignored.

Table 7. Dust resistivity (9% vol moisture, 10 ppmv SO_3)

Resistivity	Temperature (°C)		
($\Omega \cdot \text{m}$)	90	120	150
Volume	1.549×10^{12}	1.903×10^{11}	3.146×10^{10}
Surface	4.665×10^8	1.997×10^9	4.416×10^9
Acid	5.195×10^3	6.900×10^5	4.582×10^7
Total	5.195×10^3	6.898×10^5	4.528×10^7

(6) Integrated simulation of LLTESP

In engineering applications, Deutsch-Anderson equation is commonly used to calculate dust removal efficiency of ESP. The limitations of the equation are obvious, as it cannot consider the effects of various parameters, e.g., dust composition, particle size distribution, resistivity, flue gas temperature and composition.

In this model, electric field, gas flow, particle charging and particle trajectories are simulated in a coupled way. The combined effects of temperature, density, viscosity, resistivity and SO_3 condensation on

ESP are taken into account, collection efficiency for different particle sizes is obtained (Figure 24).

Temperature mainly affects particles greater than 0.1 μm . When temperature decreases, the collection efficiency for particle diameter greater than 0.1 μm improves, while the collection efficiency of particles less than 0.1 μm is barely changed. For the same particle diameter, when flue gas temperature falls from 150°C to 120°C, dust removal efficiency can increase by 0~8%. When flue gas temperature falls from 120°C to 90°C, dust removal efficiency can increase by 0~5%. It can be concluded from the integrated modelling of LLTESP, reducing flue gas temperature will increase particle collection efficiency for particle size greater than 0.1 μm , thereby increasing the total dust removal efficiency.

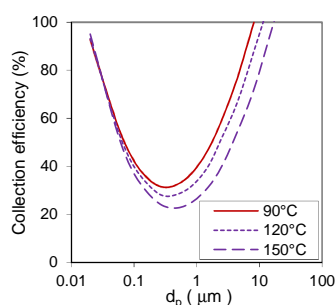


Figure 24. Combined effect of temperature on dust removal efficiency – simulation result

5. Summary and future perspective

LLTESP provides Chinese coal-fired power plants a new technique for achieving ultra-low emission with high removal efficiency for dust and SO_3 , energy saving and other significant advantages.

Laboratory and field tests have proven that, by reducing flue gas temperature, LLTESP can decrease dust resistivity, increase grading dust removal efficiency and particle charges, thus ESP outlet dust concentration has decreased significantly.

For ESP process, mathematical models for gas flow, electric field, particle charging, particle flow, back corona, dust resistivity, and SO_3 condensation are developed, finite volume method is used for the numerical simulation of LLTESP process. The major mechanisms of LLTESP in improving dust removal efficiency are revealed. When temperature is reduced from 150 °C to 90 °C, dust resistivity decreases, ESP working voltage rises, which has a significant role in improving dust removal efficiency. Adhesion of SO_3 acid condensate to the particles increases the dust dielectric constant, which has some effect on increasing saturation charge of dust particles. The collection of dust particles greater than 0.1 μm is partially improved.

Results from the experiment and numerical simulation are on the whole consistent, but there are some differences that require further investigation.

Since ESP is a complex physical process, many factors have an impact on its performance. It is difficult to rely on theoretical and experimental methods to

precisely quantify the effect of single factor. Based on fundamental physics, through accurate and quantitative computations of the governing equations of ESP process, numerical simulation technology has generated a large amount of data and information to facilitate the analysis of dust removal mechanism. With continued model development and improved accuracy, numerical simulation will be more and more valuable for the future ESP performance prediction.

References

- [1] Min Yue, Numerical simulation and study of air-flow distribution in electrostatic precipitator. Xi'an University of Technology, (2007). (In Chinese)
- [2] Bäck A., Enhancing ESP efficiency for high resistivity fly ash by reducing the flue gas temperature. 11th International Conference on Electrostatic Precipitation, Hangzhou, China, (2008), 406-412.
- [3] Noda N., Makino H., Influence of operating temperature on performance of electrostatic precipitator for pulverized coal combustion boiler, *Advanced Powder Technology*, (2010), 21, 495-499.
- [4] Guilong Xiong, Shuiqing Li, Sheng Chen, etc., Development of advanced electrostatic precipitation technologies for reducing PM2.5 emissions from coal-fired power plants. *Proceedings of the CSEE*, (2015), 35(09), 2217-2223. (In Chinese)
- [5] Porle K., Karlsson R., Kirkegaard B., Long-term experience with pulsed energization of ESP's at a Danish power station. The 6th Symposium on the Transfer and Utilization of Particulate Control Technology, New Orleans, USA, (1986).
- [6] Fujishima H., Tsuchiya Y., Onishi S., Colder side electrostatic precipitator of advanced flue gas treatment system for coal fired boiler. *ICESP VII*, Kyongju, Korea, (1998).
- [7] Zengan Liao, Study and development of low-low temperature ESP for coal fired power plants. *Applied Technology*, (2013), 10, 39-44. (In Chinese)
- [8] China Environmental Protection Industry Association-ESP Committee. China development report on electrical dust removal industry in 2013. Trade Reports. China Environmental Protection Industry. (2014). (In Chinese)
- [9] Yabe A et al., EHD study of the corona wind between wire and electrodes. *AIAA J*, (1978), 15(4), 40-345.
- [10] Yamamoto T., Velkoff H R., Electrohydrodynamics in an electrostatic precipitator. *Journal of Fluid Mechanics*, (1981), 108, 1-18.
- [11] Ushimaru K U, Butler G W., In Gas Solid Flows. *Proceedings of the 7th Annual Energy-Sources Technology Conference and Exhibition*, New Orleans, USA, (February 12-16, 1984), 87~96.
- [12] McDonald J.R., Smith W.B., Spencer III H.W., et al., A mathematical model for calculating electri-

- cal conditions in wire-duct electrostatic precipitator devices. *Appl.Phys.*, (1977), 48(6), 2231-2243.
- [13] Sekar S, Stoberg H., On the prediction of current-voltage characteristics for wire –plate precipitators. *Journal of Electrostatics*, (1981),10, 35-43
- [14] Kallio G A, Stock D E., Computation of electrical conditions inside wire-duct electrostatic precipitators using a combined finite-element and finite-difference technique. *Journal of Applied Physics*, (1985), 59, 999-1005.
- [15] Nielsen N.F., Lind L., Numerical modelling of gas distribution in electrostatic precipitators. The 8th International conference on Electrostatic Precipitation, May.15(2001).
- [16] Arrondel V., Bacchiega G., Gallimberti I., ESP Modelling: From University Studies to Industrial Application. The 8th International Conference on Electrostatic Precipitation, May.15(2001).
- [17] Hein A.G., Electrostatic Precipitation, Dust Movement and Gas flow Optimization. The 8th International Conference on Electrostatic Precipitation, May.15(2001).
- [18] Guo B.Y., Hou Q.F., Yu A.B., Li L.F., Guo J., Numerical modelling of the gas flow through perforated plates. *Chem. Eng. Res. Des.*, (2013), 91, 403-408.
- [19] Guo B.Y., Yang S.Y., Xing M., Dong K.J., Yu A.B., Guo J., Towards the development of an integrated multiscale model for electrostatic precipitation. *I&ECR*, (2013), 52, 82–93.
- [20] Guo B.Y., Guo J., Yu A.B., Simulation of the electric field in wire-plate type electrostatic precipitators. *Journal of Electrostatics*, (2014),72, 301-310.
- [21] Guo B.Y., Guo J., Yu A.B., Numerical modelling of electrostatic precipitation: Effect of gas temperature. *Journal of Aerosol Science*, (2014), 77, 102-115.
- [22] Guo B.Y., Yu A.B., Li L.F., Ye X.L., Gas-powder flow simulation in an electrostatic precipitator without electric field. Ninth Int. Conf. on CFD in the Minerals and Process Industries CSIRO, Melbourne, Australia,10-12 Dec (2012).
- [23] Lawless P.A., Sparks L.E., Measurement of ion mobilities in air and sulfur dioxide-air mixtures as a function of temperature. *Atmospheric Environment*. (1980), 14, 471-483.
- [24] Meroth A.M., Gerber T., Munz C.D., Levin P.L., et., Numerical solution of nonstationary charge coupled problems. *Electrostat.* (1999), 45, 177-198.
- [25] Lawless P.A., Particle charging bounds, symmetry relations, and an analytic charging rate model for the continuum regime. *Journal of Aerosol Science*. (1996), 7, 191-215.
- [26] Ounis H., Ahmadi G., McLaughlin J.B., Brownian diffusion of submicrometer particles in the viscous sublayer. *Journal of Colloid and Interface Science*, (1991), 143, 266–277.
- [27] Chung T.H., Lee L.L., Starling K.E., Application of kinetic gas theory and multiparameter correlation for prediction of dilute gas viscosity and thermal conductivity. *Ind. Eng. Chem. Fundamen.* (1984), 23, 8-13.
- [28] Bickelhaupt R.E., Atechnique for Predicting Fly Ash Resitivity, EPA-600/7-79-204, (1979).
- [29] Spencer H.W., Electrostatic precipitators: relationship between resitivity, particle size, and sparkover. U.S. EPA Report No.EPA-600/2-76-144, (1976).
- [30] Mclean K.J., Electric precipitators. *IEE Proceedings*. (1998), 347-361.
- [31] Shanthakumar S., Singh D.N., Phadke R.C., Flue gas conditioning for reducing suspended particulate matter from thermal power stations. *Prog Energy Combust. Sci.*, (2008), 34, 685-695.
- [32] Bayless D.J., Khan A.R., Tanneer S., Birru R., An alternative to additional SO₃ injection for fly ash conditioning, *J. Air Waste Manage Assoc* (2000), 50,169–174.
- [33] Air & Waste Management Association, *Air Pollution Engineering Manual*, (2nd ed), Ed.: W.R.Davis, Van Nostrand Reinhold, New York, USA, (1992).
- [34] Verhoff F.H., Banchemo J., Predicting dew points of flue gases. *Chem. Eng. Prog.* (1974), 70(8), 71-72.
- [35] Okkes A.G., Get Acid Dew Point of Flue Gas, *Hydrocarbon Processing*, (1987),66, 7, 53-55.
- [36] Pierce R., Estimating Acid Dewpoints in Stack Gases. *Chem. Eng.* (1977), 84, 125-128.
- [37] *Perry's Chemical Engineers' Handbook*, 7th ed., The McGraw-Hill Companies, Inc., (1997).